PROTECT Deliverable D-4.3

Amundsen Sea Embayment projections to 2050 including bedrock uncertainty

Suzanne Bevan[1], Stephen Cornford[2], Trystan Surawy-Stepney[3] and Daniel Martin[4]

[1]*Geography Department, College of Science, Swansea University, SA2 8PP, UK*

[2]*School of Geographical Sciences, University of Bristol, BS8 1SS, UK*

[3]*School of Earth and Environment, University of Leeds, LS2 9JT, UK*

[4]*Lawrence Berkeley National Laboratory, Berkeley, CA, 94720, USA*

Correspondence: Stephen Cornford <s.l.cornford@bristol.ac.uk>

1 INTRODUCTION

Current Antarctic Ice Sheet thinning is concentrated in the Amundsen Sea Embayment (ASE) sector of the West Antarctic Ice Sheet (WAIS), and in Wilkes Basin, East Antarctica (McMillan and others, 2014; Shepherd and others, 2019; Smith and others, 2020). The ASE sector contains sufficient ice above flotation height to raise global sea levels by 2.3 m (Martin and others, 2019), and between 2002 and 2013 contributed an estimated 3.2 ± 0.1 mm to total sea level rise (SLR) (Sutterley and others, 2014). Ice loss from the sector increased by a factor of 5 from the decade ending 2002 to the decade ending 2017 and has been identified as being clearly dynamic in origin (Shepherd and others, 2019) rather than being driven by surface mass balance variability. The areas that are thinning and losing mass are spreading inland, and an estimated 59% of the ASE sector was out of balance by 2016 (Shepherd and others, 2019). By this time, the two largest glaciers draining the ASE sector, Pine Island and Thwaites Glaciers, were each losing mass at rates of 55 ± 4 and 76 ± 6 Gt/a of ice, respectively. Much of the region's ice is grounded below sea level, with the ice–bedrock interface sloping inland away from the grounding line, making it potentially vulnerable to marine ice sheet instability (MISI), whereby loss of buttressing at the periphery leads to rapid and runaway grounding line retreat (Hughes, 1973; Schoof, 2007; Joughin and others, 2014). Early warning indicators of MISI show that two out of three tipping points for MISI may already have been crossed on

Pine Island Glacier, with the third tipping point, one which would lead to a total retreat of the glacier, being an increase in ocean temperatures of 1.2°C (Rosier and others, 2021).

Various studies have used stand-alone ice-sheet models to estimate contributions to future SLR from the ASE region. The modelled rates of 21st century SLR include: a modal rate value of 0.3 mm/a in an ensemble experiment calibrated with observations (Nias and others, 2019); total contributions by 2100 of 2.0 to 4.5 cm by 2100 under various ocean forcing scenarios and initialization conditions (Alevropoulos-Borrill and others, 2020); 1.5 to 4 cm by 2100 in an experiment that varied future ice-shelf melt rates and meteoric accumulation (Cornford and others, 2015); a median rise by 2100 relative to 2000 of 2 cm using different ocean forcings (Levermann and others, 2020); and a median 50 year SLR of 1.9 cm (with 90% confidence limits of 13.9 to 24.8 mm) in a study testing ensemble calibration methods (Wernecke and others, 2020). To put this into context, current observed, 2006–2018, rates of global SLR are 3.69 mm/a (3.21–4.177 mm/a) (Fox-Kemper and others, 2021) meaning that estimates of ASE near-future contributions are of the order of 10% of the global rate.

In considering global and local impacts of, and adaptations to, rising sea levels Aschwanden and others (2021) and Durand and others (2022) emphasise the need for a realistic quantification of the uncertainty associated with SLR predictions. Identifying the sources of uncertainty will, further, allow efforts to reduce them to be directed more effectively. In this report we consider the uncertainties in predicted SLR from the ASE region associated with the specification of basal conditions in the BISICLES ice-sheet model. In particular we consider different parameter values in a regularized Coulomb friction law, and random perturbations to bedrock topography.

2 MODEL SET UP

2.1 BISICLES model

We use the BISICLES ice-flow model (Cornford and others, 2015) to simulate the evolution of the ASE sector of the Antarctic ice sheet to the year 2050. BISICLES is a finite-volume model that incorporates longitudinal and lateral stresses and a simplified treatment of vertical shear based on Schoof and Hindmarsh (2010). AMR allows the spatial and temporal resolution to be fine in the locality of grounding lines and coarser elsewhere, and to evolve with grounding line migration. BISICLES meshes are constructed from rectangular patches, each of each of which is is a grid of square cells 4km, 2km, 1km, or 500m across. (Fig. 1).

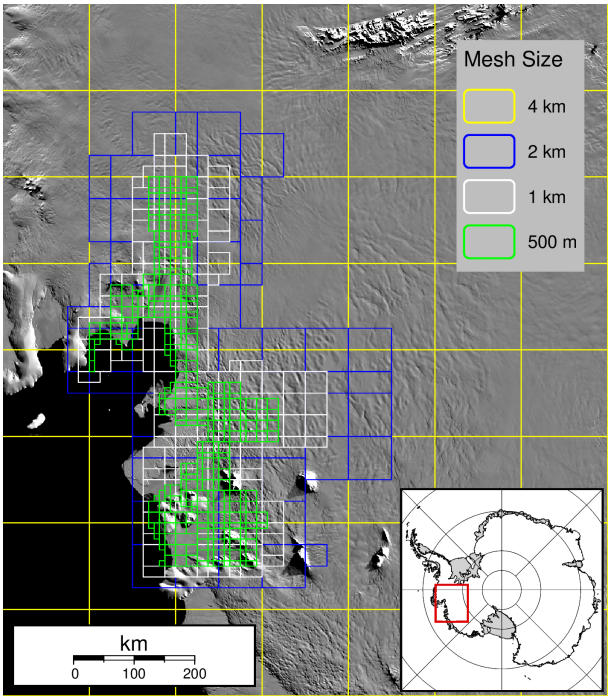

Fig. 1. Model domain and nested mesh regions.

Initial-state datasets include bedrock and surface elevation, and ice thickness from MEaSUREs BedMachine Antarctica Version 2 (Morlighem and others, 2020), and a three-dimensional temperature dataset (Pattyn, 2010). Surface accumulation rates are held constant throughout, either at 0.3 m everywhere or the mean of the monthly values from 1981 to 2018 from the Modèle Atmosphérique Régional (MAR) version 3.10 regional climate model (Agosta and others, 2019) (Fig. 2).

Ice-shelf melt rates are imposed indirectly by setting an ice-shelf thinning rate $\partial h/\partial t\,(\Omega_f) > 0$, allowing direct comparison with observations, and avoiding the need to invent depth-dependent melt-rate parameterizations. The imposition of $\partial h/\partial t\,(\Omega_f) > 0$ could represent either anomalous melt by the ocean or a weakening as a result of ice-shelf damage.

In addition, at monthly intervals between January 2016 and November 2021 we specify an ice front based on observations (Fig. 3). The full ice front corresponds to the MEaSUREs V2 coastline (Mouginot and others, 2017), Pine Island Glacier fronts are adjusted to the observed locations on 01/01/2015, 24/09/2017, 31/10/2018 and 11/02/2020, and Thwaites Glacier fronts are at monthly intervals based on a convolutional neural network applied to Sentinel-1 SAR backscatter images.

The formulation of the model requires that a stiffening coefficient (φ) and a basal traction coefficient (C) are defined by solving an inverse problem (Cornford and others, 2015). The inverse problem minimizes a

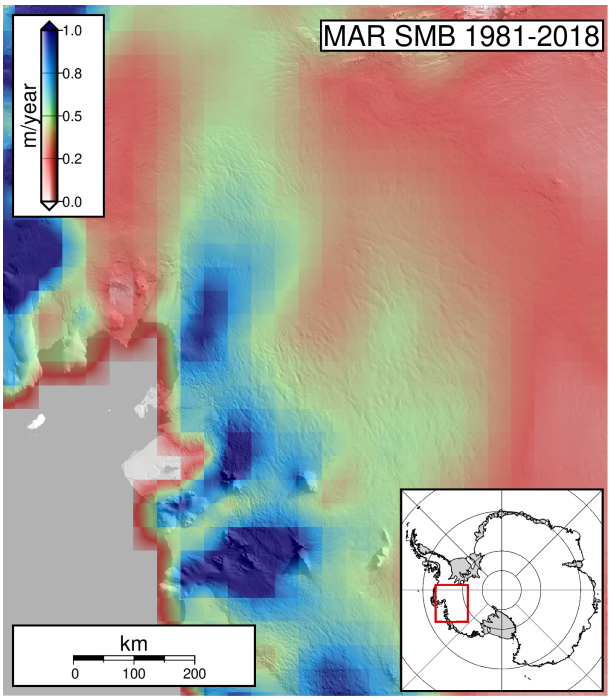

Fig. 2. Mean 1981–2018 Modèle Atmosphérique Régional (MAR) version 3.10 surface mass balance.

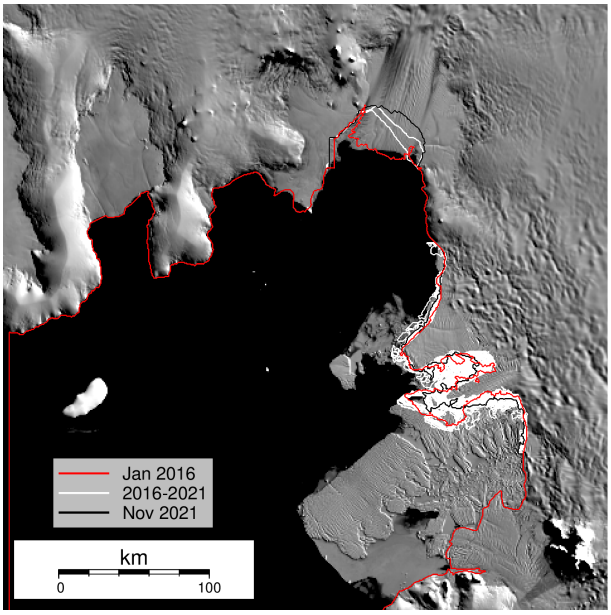

Fig. 3. Ice front positions based on satellite observation, 2016 to 2021.

cost function to create smooth continuous fields of φ and $\tau^b = C\,|\mathbf{u}|$, that produce the best match between modelled and observed ice speeds. The observed ice speeds used for the inversion are the MEaSUREs InSAR-Based Antarctica Ice Velocity Map, Version 2 (Rignot and others, 2011; Mouginot and others, 2012); those for the ASE region are based mostly on data acquired in 2007.

The stiffening coefficient is applied to the vertically integrated effective viscosity to compensate for uncertainties in ice temperature, uncertainties in the rate factor in Glen's flow law, and large-scale damage. The complete model initial state comprises ice thickness h, C, and φ, which should be consistent in the sense that the initial $\mathbf{u}$ and $\partial h/\partial t\,(\Omega_f)$ are consistent with observations. Simply taking h to be the BedMachine V2 ice thickness results in (subtle) changes to the ice geometry that lead over a few years to substantial reduction in ice flow. To address this, the grounded ice thickness is relaxed over 10 years with the ice-shelf thickness held constant and C and φ periodically recomputed.

Using the optimal φ and C coefficients and the relaxed geometry, we run the model to the year 2050, defining the start year to be 2007 and imposing the calving-front retreats described above between 2016 and 2021. For these runs we switch to a regularized Coulomb friction law (Joughin and others, 2019):

$$\tau^b = -C_{u_0}\left(\frac{|\mathbf{u}|}{|\mathbf{u}| + u_0}\right)^{1/3} \tag{1}$$

This formulation of the friction law allows friction to transition towards a plastic Coulomb law at sliding velocities $\gg u_0$, i.e. for fast-flowing ice streams and glaciers with soft deformable sediments at the bed. (Advised by Protect Technical Document D-3.1 for multi-decennial-scale modelling in Antarctica where fast-sliding ice streams are present.)

The C field produced during initialization is reformulated as C_{u_0}, to use with the regularized law:

$$C_{u_0} = C_{1/3}\left(|u|/u_0 + 1\right)^{1/3} \tag{2}$$

where

$$C_{1/3} = C\left(|u| + 1\right)^{2/3}. \tag{3}$$

Note that the '1' is simply regularization for regions where $|u| \lesssim 1$.

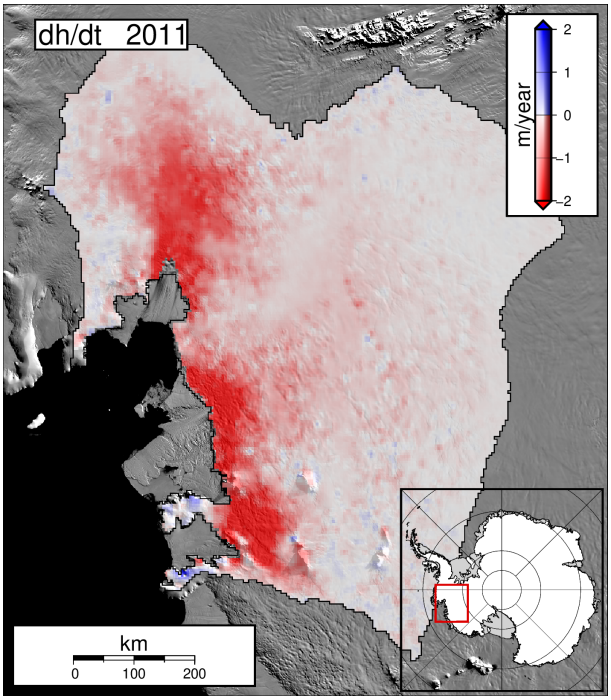

Fig. 4. 2011 observed surface elevation change.

3 OBSERVATIONS OF SURFACE ELEVATION CHANGE

Observed surface elevation change rates are based on the dataset contributed to Protect WP4-Task1.1 in which annual dh/dt rates were computed over 3-year periods using data from ERS-1/2, ENVISAT and CryoSat-2, and cover 1992 to 2017. The method used for the derivation of this dataset is described in Shepherd and others (2019).

The sea-level equivalent (SLE) of loss of volume of ice above floatation was calculated within the Thwaites Glacier and Pine Island Glacier drainage basins (basins 21 and 22 in Zwally and others (2012)). The modelled elevation changes were also masked to select only regions covered by the observed dataset (e.g. Fig. 4), and both observed and modelled volume losses were converted to sea-level equivalent (SLE) using an ice density of 917 kg/m^3.

4 ENSEMBLE SIMULATIONS

4.1 Investigating u_0 and $\partial h/\partial t\,(\Omega_f)$

Using the 0.3 m/a SMB we created a set of 45 simulations with u_0 values of 20, 75, 150, 300, 600, 1200, 2400, 3600 and 10000 m/a, each with $\partial h/\partial t\,(\Omega_f)$ values of 0, 2, 5, 10 and 15 m/a.

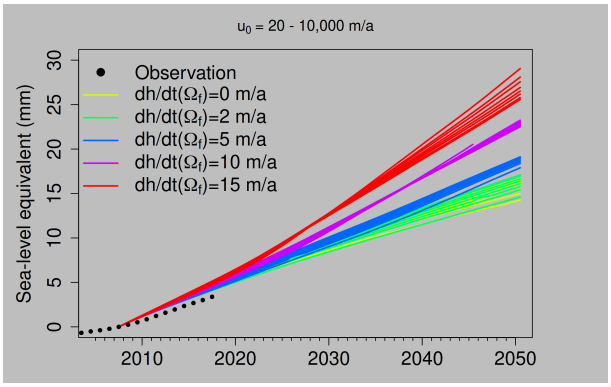

Fig. 5. Sea-level equivalent of loss of ice above floatation for u_0 ranging from 20 m/a to 10,000 m/a, coloured by the imposed rate of thinning of floating ice ($\partial h/\partial t\,(\Omega_f)$).

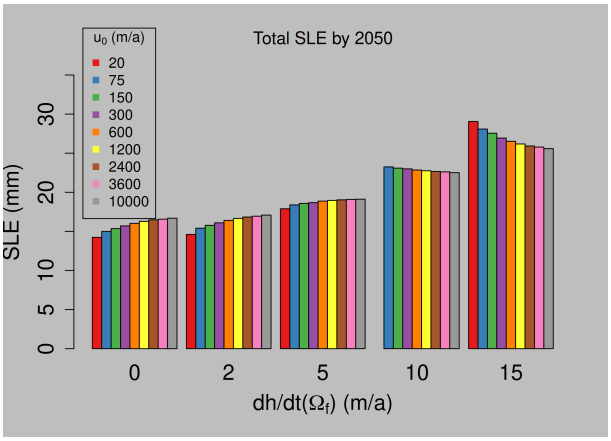

Fig. 6. Total sea-level equivalent of loss of ice above floatation for varying u_0 values, grouped by the imposed rate of thinning of floating ice ($\partial h/\partial t\,(\Omega_f)$).

The loss of ice volume above floatation by 2050 expressed in SLE varies from 14.2 mm to 29.1 mm across the full range of u_0 and $\partial h/\partial t\,(\Omega_f)$ values (Fig. 5). The greatest losses arise from high (15 m/a) rates of ice-shelf thinning, with the highest loss arising when u_0 is set to 20 m/a (Fig. 6). The correlation between the magnitude of u_0 and the total SLE switches sign between $\partial h/\partial t\,(\Omega_f) = 5$ m/a and $\partial h/\partial t\,(\Omega_f) = 10$ m/a (Fig. 6).

Figure 6 indicates that greater bed plasticity leads to greater sensitivity to loss of buttressing. At higher shelf thinning rates, greater overall volume loss is seen when u_0 is lower; that is, when a larger portion of the ice experiences plastic, Coulomb-like drag. At lower thinning rates, the converse is true. In the higher melt rate simulations, the ice tends to flow faster, with the speed increase limited more by the increasing basal traction in Weertman-like cases (large u_0). At lower thinning rates, the ice tends to slow down, and

in these cases the speed decrease is limited more by the decreasing basal traction on Weertman-like models. In everyday terms, the higher u_0, the more the bed will both increase its grip on the ice as it accelerates, and decrease its grip when the ice slows.

4.2 Simulations with perturbed bedrock

In order to investigate uncertainties in modelled ice flow relating to bedrock errors, the BedMachine bedrock elevation was perturbed with random amounts of noise following the methodology of Sun and others (2014) who applied random distributions of noise at low, medium and high frequencies to the Bedmap2 bedrock elevations in three regions of Antarctica, including the Pine Island Glacier catchment. The amplitude of the noise was determined by the uncertainty estimates accompanying the Bedmap2 dataset ($\pm$60m for the Pine Island Glacier catchment). Guided by Sun and others (2014) who found that the lowest frequency noise, equivalent to a spatial wavelength of about 8 km, had the most effect on grounding-line evolution and change in volume of ice above floatation, we added noise at frequencies equivalent to spatial wavelengths of 4, 8, 16 and 32 km. The noise was generated by using a Gaussian filter on iterations of white noise with a standard deviation of 30 m which is the reported error for BedMachine V2 over most of the fast moving ice of the ASE region. Post-filtered noise was scaled to maintain the 30 m standard deviation. We created 9 iterations of noise for each of the 4 wavelengths (e.g. Fig. 7).

The 36 iterations of noise were added to the bedrock topography in model runs using SMB = 0.3 m/a, u_0 = 300 m/a and $\partial h/\partial t\,(\Omega_f)$ values of 0, 5, and 15 m/a. The noise was also subtracted from the thickness in order to maintain surface elevations, and where applying the noise would have created negative thickness values the thickness was set to zero. The noise was also adjusted to preserve the initial grounding lines.

Adding iterations of random noise with spatial scales of 4 to 32 km to model runs with u_0 = 300 m/a produced noticeable spread in the 2050 total SLE ice loss (Fig. 8). However, the rate of thinning of floating ice has a larger impact on the magnitude of ice loss. Although not all 9 iterations completed in every case, which contributed in particular to the low standard deviation (0.3 mm) of SLE in the 16 km noise run with 15 m/a of thinning, there is a tendency for the spread, and hence uncertainty, of final SLE to increase as the spatial scale of the perturbations increases. This result confirms the findings of Sun and others (2014), that large coherent areas of bedrock uncertainty and their location, have a greater impact than small-scale noise.

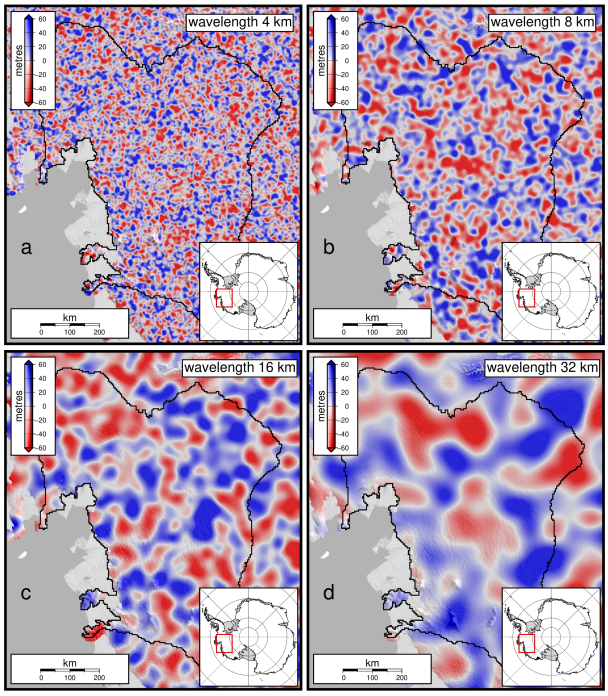

Fig. 7. Sample bedrock perturbations of wavelengths a) 4 km, b) 8 km, c) 16 km, and d) 32 km. Drainage basin outlines from Zwally and others (2012).

4.3 Mean MAR SMB simulations

Repeating the earlier simulations for the non-perturbed bedrock, described in Section 4.1 (excluding the two highest values of u_0) but using the mean MAR SMB instead of 0.3 m/a gives an insight into the effect of SMB forcing on the ice-sheet dynamics. The mean MAR SMB integrated over the Thwaites and Pine Island Glacier drainage basins, is about 30% larger than the 0.3 m/a everywhere used for the initial runs: 183 Gt compared with 122 Gt. If removing this difference, summed over the model run time, produces the same SLE as the SMB = 0.3 m/a runs then it can be concluded that the extra SMB has no effect on the ice-sheet dynamics. Figure 9 shows that for u_0=300 m/a, and $\partial h/\partial t\,(\Omega_f)$ = 0, 5, and 15 m/a, the additional SMB results in an approximately 10% increase in dynamically driven discharge. For example, with a $\partial h/\partial t\,(\Omega_f)$ = 15 m/a, removing the cumulative integrated difference between the mean MAR SMB and SMB = 0.3 m/a from the SLE produced by the MAR SMB, changes the MAR SMB SLE from 22.2 mm to 28.7 mm, 1.8 mm more than the SMB = 0.3 m/a run.

Figure 10 shows the 2050 SLE of ice loss according to u_0 and $\partial h/\partial t\,(\Omega_f)$. The black portions of the bars represent the additional dynamic component of SLE that results from the extra accumulation provided by the mean MAR SMB compared with SMB = 0.3 m/a everywhere. The increased velocities when using the

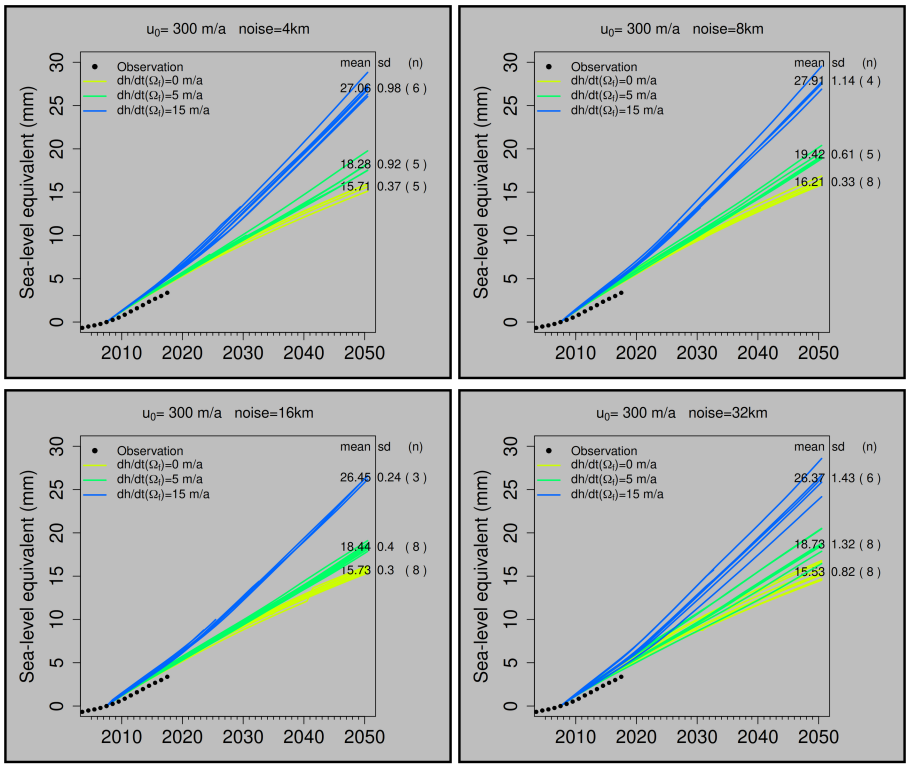

Fig. 8. Sea-level equivalent of loss of ice above floatation for $u_0 = 300$ m/a, ice-shelf thinning rates ($\partial h/\partial t\,(\Omega_f)$) of 0, 5 and 15 m/a, and bedrock elevations with different spatial-scale noise. The black dots are the SLE of the change in ice volume above floation based on the altimetry observations.

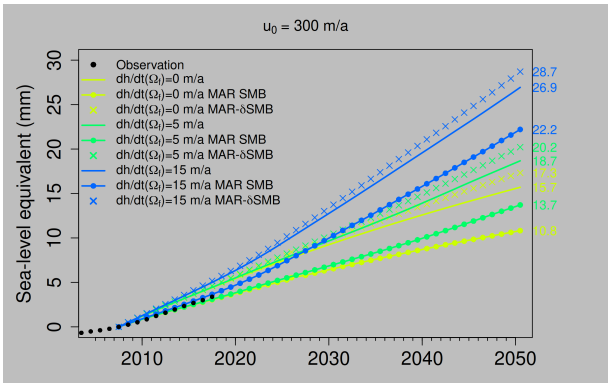

Fig. 9. Sea-level equivalent of loss of ice above floatation for varying u_0 = 300 m/a, for the SMB = 0.3 m/a simulations (solid lines) and the mean MAR SMB simulations (dotted lines). The crosses indicate SLE for the mean MAR SMB simulations minus the excess SMB compared with the SMB = 0.3 m/a simulations.

mean MAR SMB are concentrated over the areas of fast ice flow (Fig. 11).

4.4 Uncertainties arising from the C_{u_0} and φ coefficients

Next we created an ensemble to test the impact of uncertainties in the C_{u_0} and φ coefficients. We used the MAR SMB, the lowest 5 values of u_0 (as these produced the greatest variability in SLE), all 5 values of $\partial h/\partial t\,(\Omega_f)$, and for each combination of u_0 and $\partial h/\partial t\,(\Omega_f)$, we scaled each of the optimal C_{u_0} and φ coefficients by factors of 0.9 and by 1.1. This sampling generated another 100 parameter sets and outcomes. Then, using a maxmin Latin Hyercube Sampling, a further set of 64 simulations was designed, subsampling the 4-dimensional parameter space defined by all of the above values of $\partial h/\partial t\,(\Omega_f)$ = (0, 2, 5, 10 and 15 m/a), and u_0 = (20, 75, 150, 300 and 600 m/a), and C and φ coefficient factors between 0.9 and 1.1.

This ensemble resulted in the histogram and probability density shown in Fig. 12. The probability density function uses a Gaussian kernel density estimator with a Silverman rule-of-thumb bandwidth (Silverman, 1986). The mean SLE of the ensemble of runs is 17.8 mm. The 5th and 95th percentiles of the probability density function are -0.7 and 41.0 mm SLE, respectively, the median value is 16.1 mm, and the modal value is 10.0 mm.

The extrapolated observation-based SLE of 15.4 mm by 2050, is based on the mean rate of observed volume change between 2007 and 2017. Both the mean and the median of the model ensemble are only marginally above the extrapolation of observed change. The next steps will be to use spatial observations of dh/dt and ice velocity change to reduce the credibility interval of the simulated SLE outcomes.

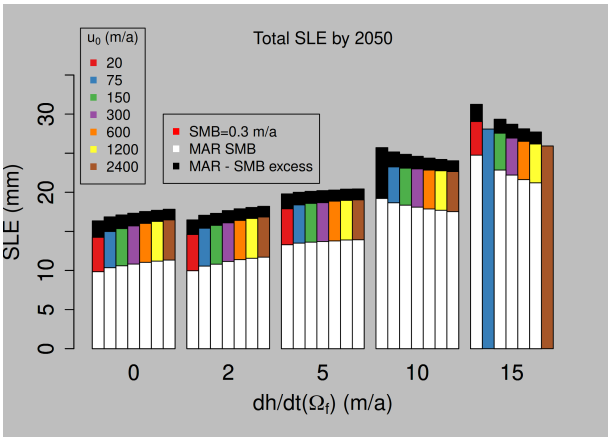

Fig. 10. Total sea-level equivalent of loss of ice above floatation for varying u_0 values, grouped by the imposed rate of thinning of floating ice ($\partial h/\partial t\,(\Omega_f)$). The white bars show the SLE using the mean MAR SMB, the coloured bars show the SLE for SMB = 0.3 m/a, and the black sections shows the SLE ice loss after the (MAR - 0.3 m/a) excess accumulation has been removed from the MAR SMB simulations.

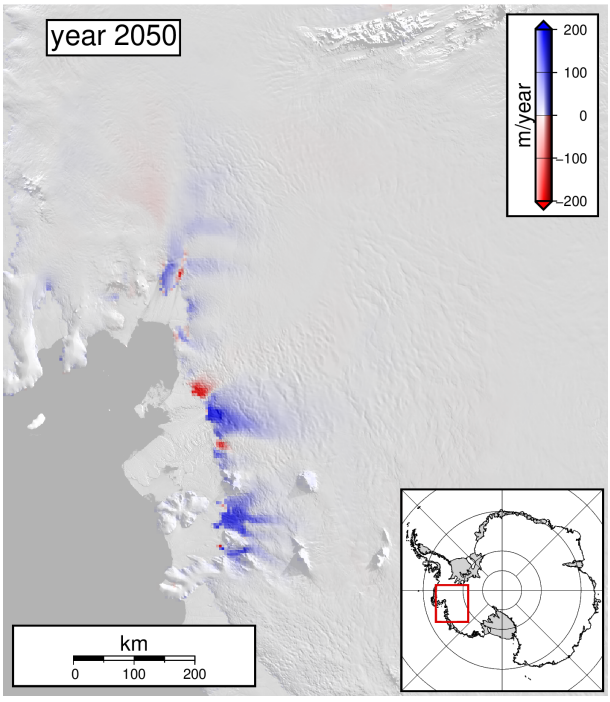

Fig. 11. Change in ice velocity by 2050 between a simulation forced with the mean MAR SMB compared with one using an SMB of 0.3 m/a everywhere. Both simulations were run with $u_0 = 300$ m/a and $\partial h/\partial t\,(\Omega_f) = 15$ m/a.

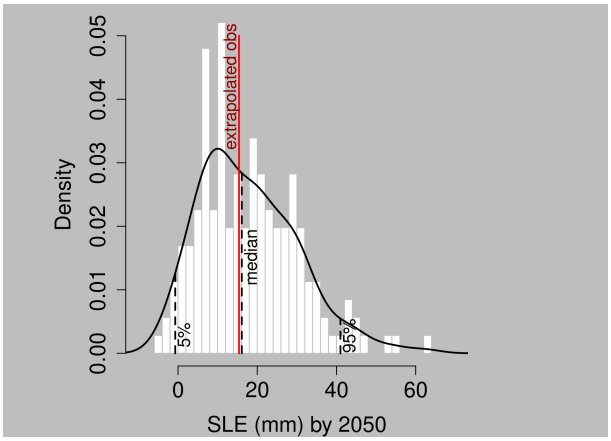

Fig. 12. Histogram and density function of the MAR SMB ensemble. The 5th and 95th percentiles, and the median of the density function are indicated with vertical dashed lines. The vertical red line shows the mean 2007–2017 rate of observed SLE volume loss extrapolated to 2050.

5 DELIVERED DATASETS

We have made available 1 km resolution output data files for each year, 2007 to 2052, of a single randomly selected simulation from each of the 30 histogram breaks in Fig. 12. The datasets follow the ISMIP6 naming protocol (`https://www.climate-cryosphere.org/wiki/index.php?title=ISMIP6-Projections-Antarctica#A2.3_Model_output_variables_and_README_file`). We include state variables lithk, orog, sftflf, sftgif, sftgrf, strbasemag, topg, uvelmean, vvelmean, fluxes licalvf, ligroundf, and scalars lim, limnsw, iareagr, iareafl, tendacabf, tendlibmassbf, tendlicalvf, tendligroundf and tendligroundf. Each NetCDF file is named according to the variable, the simulation parameters and the 2050 SLE value. For example orog_ASE_BISICLES.uj_20.dl is the orography data for simulation u_0=20 m/a, $\partial h/\partial t\,(\Omega_f) = 5$ m/a, C scaled by 0.9, φ scaled by 0.9, and a final SLE of 43.06 mm. See Table 1 for the full list which includes the SLE of ice mass loss for each simulation.

Table 1. Delivered datasets

Name	u_0	$\partial h/\partial t\,(\Omega_f)$	C	φ	SLE
	m/a	m/a	scaling	scaling	mm
*_ASE_BISICLES.uj_20.dhfdt_0.C_1.10.phi_1.10.slr_-4.44	20	0	1.10	1.10	-4.44
*_ASE_BISICLES.uj_20.dhfdt_0.C_1.08.phi_1.10.slr_-2.70	20	0	1.08	1.10	-2.70
*_ASE_BISICLES.uj_20.dhfdt_5.C_1.10.phi_1.10.slr_-0.69	20	5	1.10	1.10	-0.69
*_ASE_BISICLES.uj_20.dhfdt_2.C_1.07.phi_1.05.slr_0.43	20	2	1.07	1.05	0.43
*_ASE_BISICLES.uj_150.dhfdt_5.C_1.10.phi_1.10.slr_2.55	150	5	1.10	1.10	2.55
*_ASE_BISICLES.uj_20.dhfdt_2.C_1.10.phi_0.90.slr_4.03	20	2	1.10	0.90	4.03
*_ASE_BISICLES.uj_20.dhfdt_0.C_1.02.phi_1.00.slr_7.26	20	0	1.02	1.00	7.26
*_ASE_BISICLES.uj_20.dhfdt_2.C_1.00.phi_1.00.slr_9.97	20	2	1.00	1.00	9.97
*_ASE_BISICLES.uj_600.dhfdt_2.C_1.00.phi_1.00.slr_11.39	600	2	1.00	1.00	11.39
*_ASE_BISICLES.uj_20.dhfdt_5.C_1.00.phi_1.00.slr_13.29	20	5	1.00	1.00	13.29
*_ASE_BISICLES.uj_600.dhfdt_10.C_1.11.phi_0.92.slr_14.31	600	10	1.11	0.92	14.31
*_ASE_BISICLES.uj_600.dhfdt_2.C_0.90.phi_1.10.slr_17.66	600	2	0.90	1.10	17.66
*_ASE_BISICLES.uj_300.dhfdt_5.C_0.94.phi_1.02.slr_18.31	300	5	0.94	1.02	18.31
*_ASE_BISICLES.uj_150.dhfdt_2.C_0.90.phi_1.10.slr_20.31	150	2	0.90	1.10	20.31
*_ASE_BISICLES.uj_300.dhfdt_15.C_1.00.phi_1.00.slr_22.20	300	15	1.00	1.00	22.20
*_ASE_BISICLES.uj_600.dhfdt_0.C_0.90.phi_0.90.slr_24.84	600	0	0.90	0.90	24.84
*_ASE_BISICLES.uj_300.dhfdt_0.C_0.90.phi_0.90.slr_26.38	300	0	0.90	0.90	26.38
*_ASE_BISICLES.uj_300.dhfdt_15.C_0.90.phi_1.10.slr_29.24	300	15	0.90	1.10	29.24
*_ASE_BISICLES.uj_75.dhfdt_15.C_0.97.phi_0.97.slr_30.67	75	15	0.97	0.97	30.67
*_ASE_BISICLES.uj_150.dhfdt_10.C_0.93.phi_0.92.slr_33.50	150	10	0.93	0.92	33.50
*_ASE_BISICLES.uj_20.dhfdt_15.C_0.99.phi_0.92.slr_34.21	20	15	0.99	0.92	34.21
*_ASE_BISICLES.uj_300.dhfdt_10.C_0.90.phi_0.90.slr_36.65	300	10	0.90	0.90	36.65
*_ASE_BISICLES.uj_600.dhfdt_15.C_0.90.phi_0.90.slr_38.93	600	15	0.90	0.90	38.93
*_ASE_BISICLES.uj_20.dhfdt_0.C_0.90.phi_0.90.slr_41.11	20	0	0.90	0.90	41.11
*_ASE_BISICLES.uj_300.dhfdt_15.C_0.90.phi_0.90.slr_42.09	300	15	0.90	0.90	42.09
*_ASE_BISICLES.uj_75.dhfdt_10.C_0.90.phi_0.90.slr_45.02	75	10	0.90	0.90	45.02
*_ASE_BISICLES.uj_150.dhfdt_15.C_0.90.phi_0.90.slr_46.76	150	15	0.90	0.90	46.76
*_ASE_BISICLES.uj_75.dhfdt_15.C_0.90.phi_0.90.slr_52.10	75	15	0.90	0.90	52.10
*_ASE_BISICLES.uj_20.dhfdt_10.C_0.90.phi_0.90.slr_54.95	20	10	0.90	0.90	54.95
*_ASE_BISICLES.uj_20.dhfdt_15.C_0.90.phi_0.90.slr_62.33	20	15	0.90	0.90	62.33

REFERENCES

Agosta C, Amory C, Kittel C, Orsi A, Favier V, Gallée H, van den Broeke MR, Lenaerts JTM, van Wessem JM, van de Berg WJ and Fettweis X (2019) Estimation of the Antarctic surface mass balance using the regional climate model MAR (1979–2015) and identification of dominant processes. *The Cryosphere*, **13**(1), 281–296, ISSN 1994-0416 (doi: 10.5194/tc-13-281-2019)

Alevropoulos-Borrill AV, Nias IJ, Payne AJ, Golledge NR and Bingham RJ (2020) Ocean-forced evolution of the Amundsen Sea catchment, West Antarctica, by 2100. *The Cryosphere*, **14**(4), 1245–1258, ISSN 1994-0416 (doi: 10.5194/tc-14-1245-2020)

Aschwanden A, Bartholomaus TC, Brinkerhoff DJ and Truffer M (2021) Brief communication: A roadmap towards credible projections of ice sheet contribution to sea level. *The Cryosphere*, **15**(12), 5705–5715, ISSN 1994-0416 (doi: 10.5194/tc-15-5705-2021)

Cornford SL, Martin DF, Payne AJ, Ng EG, Brocq AML, Gladstone RM, Edwards TL, Shannon SR, Agosta C, Broeke MRvd, Hellmer HH, Krinner G, Ligtenberg SRM, Timmermann R and Vaughan DG (2015) Century-scale simulations of the response of the West Antarctic Ice Sheet to a warming climate. *The Cryosphere*, **9**(4), 1579–1600, ISSN 1994-0416 (doi: 10.5194/tc-9-1579-2015)

Durand G, van den Broeke MR, Le Cozannet G, Edwards TL, Holland PR, Jourdain NC, Marzeion B, Mottram R, Nicholls RJ, Pattyn F, Paul F, Slangen ABA, Winkelmann R, Burgard C, van Calcar CJ, Barré JB, Bataille A and Chapuis A (2022) Sea-Level Rise: From Global Perspectives to Local Services. *Frontiers in Marine Science*, **8**, ISSN 2296-7745

Fox-Kemper B, Hewitt H, Xiao C, Aðalgeirsdóttir G, Drijfhout S, Edwards T, Golledge N, Hemer N, Kopp R, Krinner G, Mix A, Notz D, Nowicki S, Nurhati I, Ruiz L, Sallée JB, Slangen A and Yu (2021) Ocean, Cryosphere and Sea Level Change. In V Masson-Delmotte, P Zhai, A Pirani, S Connors, C Péan, S Berger, N Caud, Y Chen, L Goldfarb, M Gomis, M Huang, K Leitzell, E Lonnoy, J Matthews, T Maycock, T Waterfield, O Yelekçi, R Yu and B Zhou (eds.), *Climate Change 2021: The Physical Science Basis. Contribution of Working Group I to the Sixth Assessment Report of the Intergovernmental Panel on Climate Change*, 1211–1362, Cambridge University Press, Cambridge, United Kingdom and New York, NY, USA

Hughes T (1973) Is the west Antarctic Ice Sheet disintegrating? *Journal of Geophysical Research*, **78**(33), 7884–7910, ISSN 2156-2202 (doi: 10.1029/JC078i033p07884)

Joughin I, Smith BE and Medley B (2014) Marine Ice Sheet Collapse Potentially Under Way for the Thwaites Glacier Basin, West Antarctica. *Science*, **344**(6185), 735–738, ISSN 1095-9203 (doi: 10.1126/science.1249055)

Joughin I, Smith BE and Schoof CG (2019) Regularized Coulomb Friction Laws for Ice Sheet Sliding: Application to Pine Island Glacier, Antarctica. *Geophysical Research Letters*, **46**(9), 4764–4771, ISSN 1944-8007 (doi: 10.1029/2019GL082526)

Levermann A, Winkelmann R, Albrecht T, Goelzer H, Golledge NR, Greve R, Huybrechts P, Jordan J, Leguy G, Martin D, Morlighem M, Pattyn F, Pollard D, Quiquet A, Rodehacke C, Seroussi H, Sutter J, Zhang T, Van Breedam J, Calov R, DeConto R, Dumas C, Garbe J, Gudmundsson GH, Hoffman MJ, Humbert A, Kleiner T, Lipscomb WH, Meinshausen M, Ng E, Nowicki SMJ, Perego M, Price SF, Saito F, Schlegel NJ, Sun S and van de Wal RSW (2020) Projecting Antarctica's contribution to future sea level rise from basal ice shelf melt using linear response functions of 16 ice sheet models (LARMIP-2). *Earth System Dynamics*, **11**(1), 35–76, ISSN 2190-4979 (doi: 10.5194/esd-11-35-2020)

Martin DF, Cornford SL and Payne AJ (2019) Millennial-Scale Vulnerability of the Antarctic Ice Sheet to Regional Ice Shelf Collapse. *Geophysical Research Letters*, **46**(3), 1467–1475, ISSN 00948276 (doi: 10.1029/2018gl081229)

McMillan M, Shepherd A, Sundal A, Briggs K, Muir A, Ridout A, Hogg A and Wingham D (2014) Increased ice losses from Antarctica detected by CryoSat-2. *Geophysical Research Letters*, **41**(11), 3899–3905, ISSN 1944-8007 (doi: 10.1002/2014GL060111)

Morlighem M, Rignot E, Binder T, Blankenship D, Drews R, Eagles G, Eisen O, Ferraccioli F, Forsberg R, Fretwell P, Goel V, Greenbaum JS, Gudmundsson H, Guo J, Helm V, Hofstede C, Howat I, Humbert A, Jokat W, Karlsson NB, Lee WS, Matsuoka K, Millan R, Mouginot J, Paden J, Pattyn F, Roberts J, Rosier S, Ruppel A, Seroussi H, Smith EC, Steinhage D, Sun B, Broeke MRvd, Ommen TDv, Wessem Mv and Young DA (2020) Deep glacial troughs and stabilizing ridges unveiled beneath the margins of the Antarctic ice sheet. *Nature Geoscience*, **13**(2), 132–137, ISSN 1752-0908 (doi: 10.1038/s41561-019-0510-8)

Mouginot J, Scheuchl B and Rignot E (2012) Mapping of Ice Motion in Antarctica Using Synthetic-Aperture Radar Data. *Remote Sensing*, **4**(9), 2753–2767, ISSN 2072-4292 (doi: 10.3390/rs4092753)

Mouginot J, Scheuchl B and Rignot E (2017) *MEaSUREs Antarctic Boundaries for IPY 2007-2009 from Satellite Radar, Version 2.* Boulder, Colorado, USA: NASA National Snow and Ice Data Center Distributed Active Archive Center

Nias IJ, Cornford SL, Edwards TL, Gourmelen N and Payne AJ (2019) Assessing uncertainty in the dynamical ice response to ocean warming in the Amundsen Sea Embayment, West Antarctica. *Geophysical Research Letters*, (ja), ISSN 1944-8007 (doi: 10.1029/2019GL084941)

Pattyn F (2010) Antarctic subglacial conditions inferred from a hybrid ice sheet/ice stream model. *Earth and Planetary Science Letters*, **295**(3), 451–461, ISSN 0012-821X (doi: 10.1016/j.epsl.2010.04.025)

Rignot E, Mouginot J and Scheuchl B (2011) Ice Flow of the Antarctic Ice Sheet. *Science*, **333**(6048), 1427–1430, ISSN 0036-8075 (doi: 10.1126/science.1208336)

Rosier SHR, Reese R, Donges JF, De Rydt J, Gudmundsson GH and Winkelmann R (2021) The tipping points and early warning indicators for Pine Island Glacier, West Antarctica. *The Cryosphere*, **15**(3), 1501–1516, ISSN 1994-0416 (doi: 10.5194/tc-15-1501-2021)

Schoof C (2007) Ice sheet grounding line dynamics: Steady states, stability, and hysteresis. *J. Geophys. Res.*, **112**(F3), F03S28+ (doi: 10.1029/2006jf000664)

Schoof C and Hindmarsh RCA (2010) Thin-Film Flows with Wall Slip: An Asymptotic Analysis of Higher Order Glacier Flow Models. *The Quarterly Journal of Mechanics and Applied Mathematics*, **63**(1), 73–114, ISSN 0033-5614 (doi: 10.1093/qjmam/hbp025)

Shepherd A, Gilbert L, Muir AS, Konrad H, McMillan M, Slater T, Briggs KH, Sundal AV, Hogg AE and Engdahl ME (2019) Trends in Antarctic Ice Sheet Elevation and Mass. *Geophysical Research Letters*, **46**(14), 8174–8183, ISSN 1944-8007 (doi: 10.1029/2019GL082182)

Silverman BW (1986) *Density Estimation for Statistics and Data Analysis*. CRC Press, ISBN 978-0-412-24620-3

Smith B, Fricker HA, Gardner AS, Medley B, Nilsson J, Paolo FS, Holschuh N, Adusumilli S, Brunt K, Csatho B, Harbeck K, Markus T, Neumann T, Siegfried MR and Zwally HJ (2020) Pervasive ice sheet mass loss reflects competing ocean and atmosphere processes. *Science*, ISSN 0036-8075, 1095-9203 (doi: 10.1126/science.aaz5845)

Sun S, Cornford SL, Liu Y and Moore JC (2014) Dynamic response of Antarctic ice shelves to bedrock uncertainty. *The Cryosphere*, **8**(4), 1561–1576, ISSN 1994-0416 (doi: 10.5194/tc-8-1561-2014), publisher: Copernicus GmbH

Sutterley TC, Velicogna I, Rignot E, Mouginot J, Flament T, van den Broeke MR, van Wessem JM and Reijmer CH (2014) Mass loss of the Amundsen Sea Embayment of West Antarctica from four independent techniques. *Geophysical Research Letters*, **41**(23), 8421–8428, ISSN 1944-8007 (doi: 10.1002/2014GL061940)

Wernecke A, Edwards TL, Nias IJ, Holden PB and Edwards NR (2020) Spatial probabilistic calibration of a high-resolution Amundsen Sea Embayment ice sheet model with satellite altimeter data. *The Cryosphere*, **14**(5), 1459–1474, ISSN 1994-0416 (doi: 10.5194/tc-14-1459-2020)

Zwally HJ, Giovinetto MB, Beckley MA and Saba JL (2012) *Antarctic and Greenland Drainage Systems*. GSFC Cryospheric Sciences Laboratory (doi: https://earth.gsfc.nasa.gov/cryo/data/polar-altimetry/antarctic-and-greenland-drainage-systems)